## Chemical Geology 587 (2022) 120629



Contents lists available at ScienceDirect

## Chemical Geology

journal homepage: www.elsevier.com/locate/chemgeo





## Persistence of old soil carbon under changing climate: The role of mineral-organic matter interactions

Katherine E. Grant <sup>a,\*</sup>, Valier V. Galy <sup>b</sup>, Negar Haghipour <sup>c,d</sup>, Timothy I. Eglinton <sup>c</sup>, Louis A. Derry <sup>a,e</sup>

- <sup>a</sup> Department of Earth and Atmospheric Sciences, Cornell University, Ithaca, NY 14853, USA
- b Department of Marine Chemistry and Geochemistry, Woods Hole Oceanographic Institution, 266 Woods Hole Road, Woods Hole, MA 02543, USA
- <sup>c</sup> Geological Institute, ETH-Zurich, Zurich, Switzerland
- <sup>d</sup> Laboratory for Ion Beam Physics, ETH-Zurich, Zurich, Switzerland
- <sup>e</sup> Institut de Physique du Globe de Paris, France

#### ARTICLE INFO

Editor: Dr. Hailiang Dong

#### ABSTRACT

Globally, soils store between 1500 and 2800 Pg of organic carbon (OC). The physical and chemical stability of these terrestrial soil carbon stores under plausible climate change scenarios is unclear. Soil organic carbon (SOC), especially in volcanic soils, is stabilized through mineral matrix interactions. How susceptible are these mineralorganic matter interactions to environmental change? Here we present a study of SOC age along a climate gradient of andisols from Kohala volcano on the Island of Hawai'i. We measure carbon isotope composition  $(^{14}\text{C}/^{12}\text{C}, \, ^{13}\text{C}/^{12}\text{C})$  in bulk samples and extracted biomarkers for 4–8 horizons of 15 soil profiles to understand variability in SOC age and persistence across incremental differences in mean annual precipitation. Bulk OC in the subsoil has radiocarbon fraction modern (Fm) values as low as 0.28 to 0.16 (~10.160 to ~14.630 conventional radiocarbon years). Coexisting plant-derived long chain fatty acids (LCFAs) are older, over 22,500 yrs. (Fm = 0.060), implying that these are among the most stable compounds in the soil, while corresponding shorterchain (C16) fatty acids are much younger, consistent with an origin from active microbial communities assimilating young OC percolating from surface horizons. There is significant Fe loss at higher mean annual precipitation (MAP) (>2200 mm yr $^{-1}$ ) sites associated with episodic soil saturation and microbial Fe reduction. %OC is higher at these sites, consistent with the expectation that saturated conditions promote SOC storage. However, in these higher MAP sites iron depletion is associated with much younger bulk SOC and LCFAs  $^{14}$ C ages ( $\sim$ 2900  $^{14}$ C years) than at equivalent sample depths in sites that retain most Fe ( $\sim$ 14,200  $^{14}$ C years). The remaining mineral matrix consists primarily of Si, Al, and Ti as SRO minerals. The data imply that modest increases in precipitation resulting from environmental change at locations near a potential saturation or redox threshold could result in destabilization of Fe-SOC complexes, rendering previously stabilized carbon available for rapid degradation, potentially irreversibly decreasing the size of the old SOC reservoir. The destabilization of an old, persistent Fe-SOC reservoir can decrease SOC storage and ultimately increase the amount of CO2 released to the atmosphere.

## 1. Introduction

Soils store and actively exchange carbon with the atmosphere, plants, and hydrologic system. In the tropics, much of this rapidly exchanging C is produced and stored in living, above ground biomass (Saatchi et al., 2011), and a significant fraction of this terrestrial net primary productivity ( $\approx$ 60 Pg yr<sup>-1</sup>, (Beer et al., 2010)) enters soils. The size of the global soil C reservoir is uncertain but has been estimated to

be 1500 to 2800 Pg (Scharlemann et al., 2014). Volcanic soils have a particularly large capacity to store carbon due to their high reactive mineral surface area (Shoji et al., 1993). Even though volcanic soils make up less than 1% of soils globally, they account for 5% of global SOC storage (Dahlgren et al., 2004). A larger fraction (5.8%) of the Earth's surface is covered by basic to intermediate rocks and soils developed on this material may be classified as volcanic soils and contain significant SOC even if they do not meet the stricter

E-mail address: keg89@cornell.edu (K.E. Grant).

<sup>\*</sup> Corresponding author.

requirements for Andosols or Andisols (Hartmann et al., 2012).

Uncertainty in the size and stability of the SOC reservoir is partially attributed to the unknown distribution and turnover times of deep soil organic carbon (SOC), as the amount and age of C stored below 30 cm and certainly below 1 m is not well constrained (Rumpel and Kogel-Knabner, 2011). While much OC input to soils is remineralized on short time scales (<3 years; (Jenkinson and Rayner, 1977)), some SOC is persistent on millennial time scales (Torn et al., 1997; Trumbore, 2009; Lehmann and Kleber, 2015; Shi et al., 2020). Given recent and predicted anthropogenic climate change, potential destabilization of the terrestrial soil carbon stores is of increasing concern (Trumbore, 1997; Davidson and Janssens, 2006; Jackson et al., 2017). Recent studies examining riverine particulate OC as an integrated landscape-scale metric to estimate the climate control of SOC turnover indicate that increased precipitation and temperature destablize millenial aged OC (Eglinton et al., 2021, Hein et al., 2020), however direct evidence from soils remains sparse.

It is increasingly clear that the association of SOC with mineral matrices, via chemical interactions or physical protection (e.g., occlusion), plays a significant role in carbon persistence (Torn et al., 1997; Schmidt et al., 2011; Hemingway et al., 2019). Much of the "stabilized" SOC is thought to be a loose interaction between dissolved organic carbon (DOC), microbially processed OC, and partially degraded or intact plant compounds with mineral surfaces, mainly Fe-oxides (Mikutta et al., 2019; Coward et al., 2017; Kaiser and Guggenberger, 2000) which inhibits microbial degradation of the OC. In many soils, these interactions become more important below 30 cm where the mineral surfaces are more avalible and where carbon is generally older (Shi et al., 2020; He, 2016). One concern is that these mineral surface interactions that stabilize OC could be highly reversible under changing soil conditions (Schimel et al., 2011; Schmidt et al., 2011), particularly given that climate models suggest the tropics could experience increased precipitation concurrent with increases in temperature (Su et al., 2017; Feng et al., 2019). Short range order (SRO) iron minerals can be destabilized in anerobic environments where the non-crystalline Fe(III) minerals are mobilized via reductive dissolution and leached from the system (Thompson et al., 2008; Henderson et al., 2012; Buettner et al., 2014; Possinger et al., 2020). Laboratory manipulations under anaerobic conditions show that dissolution of iron oxides by chemical reduction of Fe, or by introducing known microbial Fe reducers to the incubations, can facilitate the release of OC (Pan et al., 2016; Huang and Hall, 2017; Zhao et al., 2017), however the behavior of iron and carbon in natural settings under variable redox conditions is less well known.

Soil OC studies often use bulk radiocarbon to assess and model the turnover time of SOC (Sierra et al., 2017). However <sup>14</sup>C measurements of "bulk" OC reflect a mixture of all the carbon compounds in a sample and may not reflect the true cycling of the individual pools of OC because such measurements can be readily skewed towards younger values when small amounts of newly fixed OC are input into deep soils. To overcome these limitations, different SOC pools are often distinguished according to operationally-defined fractions based on physical or chemical separations (e.g., Schrumpf et al., 2013; Poeplau et al., 2018). Increasingly, compound specific <sup>14</sup>C techniques for understanding <sup>14</sup>C variability developed for marine and riverine studies are being used in soil studies, including compound specific analysis and ramped pyrolysis/oxidation (RPO) (e.g. van der Voort et al., 2017; Grant et al., 2019; Sanderman and Grandy, 2020). Generally, lipids are found to persist longer in the environment, especially in marine DOC and sediments than carbohydrates and proteins (Loh, 2014; Wang, 1998, Lutzow et al., 2006, Rethemeyer et al., 2004). While this has not been extensively explored in soils, van der Voort et al. (2017) found that long-chain n-alkyl lipids (n-alkanoic acids, "LCFA", C24-C30) are older than the bulk soil. Gies et al. (2020) found that glycerol dialkyl glycerol tetraethers (GDGTs) membrane lipids of archaea and bacteria- in alpine mineral soil horizons were millennial in age, and reflect a stabilized pool of microbial necromass. However, all these studies use soils formed on sedimentary rock,

in temperate or sub-alpine sites where mineral-OC associations may be very different from tropical forest and grassland soils and where there is the potential for input from petrogenic radiocarbon-dead sources.

In order to directly test the influence of precipitation variability on OC residence time, we examine soil OC and <sup>14</sup>C distributions along a climate gradient, allowing us to capture the soil weathering history and examine how inherent variations may be indicative of future change. We use the Kohala climate gradient model system to test SOC persistence across a range of soil properties, including moisture, iron and carbon content, pH, mineralogy and redox status (Vitousek et al., 1997; Chadwick et al., 2003; Thompson et al., 2006a). An overall relationship between carbon persistence, soil formation, and pedogenic thresholds has been previously proposed for Kohala soils (Torn et al., 1997; Inagaki et al., 2020), but the pattern of radiocarbon age variations with depth and across changing weathering zones has not been previously established.

Here, we use a combination of bulk and compound-specific radiocarbon measurementsss to assess spatial and depth-related variations in the age and persistence of particular plant wax lipids (LCFA, C24-C30) and microbially influenced short-chain lipids (SCFAs C<sub>16</sub>-C<sub>18</sub>). The use of specific organic compounds to understand OC residence time allows us to explore the origin and persistence of OC at a molecular level, and in particular to examine microbially mediated processes leading to incorporation of modern OC into SOM (as manifested in <sup>14</sup>C values of shortchain fatty acids), and to preferential retention of plant wax lipids under contrasting environmental conditions. We have two initial and somewhat competing hypotheses about the controls on the abundance and age of SOC along the climate gradient in our study. Hypothesis 1 is that OC age and abundance will increase with increasing MAP. As MAP increases we should find increasingly saturated conditions with more frequent oxygen limitation and lower potential for decomposition. Thus, H1 predicts both bulk OC and individual lipids will have older <sup>14</sup>C ages in the high MAP soils compared to the drier, more oxidized, lower elevation soils. Hypothesis 2 is that SRO phases such as non-crystalline Fe-oxides play a dominant role in stabilizing old SOC. H2 predicts that the age of SOC will be correlated with abundance of SRO phases that do not simply scale with MAP. Thus the two hypotheses predict different controls and different patterns of SOC age and abundance along the climate gradient.

The large data set for radiocarbon and elemental chemistry across a significant range of MAP allows us to map changes in carbon content and residence time on to geochemical variations. However, since soils at any scale (e.g., micron, aggregate, core, profile, landscape) are extremely heterogeneous, we expect to see both trends spanning the gradient and local effects that are specific to certain areas of the soil environment. This "high-resolution" window on changes in SOC properties and isotopic compositions down soil depth profiles, and spanning contrasting environmental conditions, can thus be thought of as a 2-dimensional study encompassing both depth (to  $\sim 1$  m) and climate gradient.

## 2. Materials and methods

## 2.1. Site and sample description

Fifteen sites were sampled on the leeward side of Kohala Mountain on the Island of Hawaii (Fig. 1) in January 2014 and 2015 and April 2016 (Table 1). Kohala Mountain is an extinct shield volcano with multiple volcanic episodes (Spengler and Garcia, 1988). Two volcanic series, the Hawi and Pololu, make up the soil parent material on Kohala. The sites for this study are located on the older 350 ka Pololu volcanics, but there is a significant contribution of ash and tephra from the younger 150 ka Hawi series (Bullen and Chadwick, 2016; Vitousek and Chadwick, 2013). The magmatic evolution from the Pololu sequence to the Hawi sequence significantly changed the inorganic geochemistry of the resulting basalts, increasing Nb concentrations by a factor of 10 while TiO<sub>2</sub> varied only by a factor of 3. We use the TiO<sub>2</sub>/Nb ratio to understand

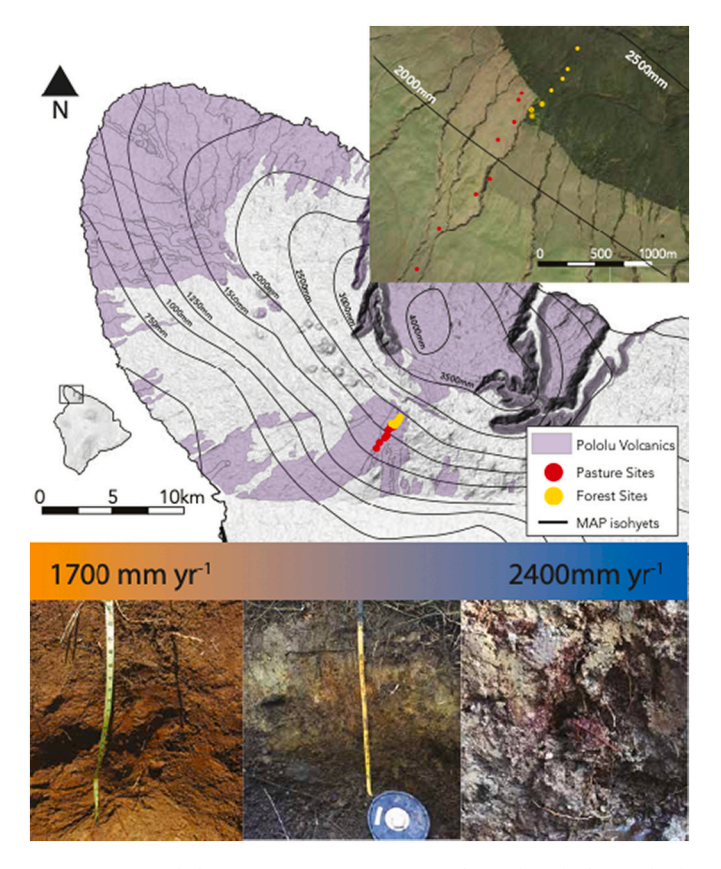


**Fig. 1.** Map of Kohala Mountain, Hawai'i. Sites are located on the leeward side of the mountain on the 350 ka Pololu lava flow. Soil were collected from 15 sites across a climate gradient ranging from 1500 mm to 2400 mm rainfall/year. The shaded purple areas are the exposed Pololu lavas, where the grey is the overlying Hawi (150 ka) flows. The black lines indicate MAP isohyets generated by the Hawaii Rainfall Database (Giambelluca and Sanderson, 2013). The 15 sites span the forest/pasture conversion boundary, with 8 pasture sites (red symbols) and 7 forest sites (yellow symbols). Some pasture and forest sites overlap in elevation. (For interpretation of the references to color in this figure legend, the reader is referred to the web version of this article.)

the mixed provenance of parent material in the sites sampled since this ratio does not change during weathering and provides a direct reflection of the magmatic history.  $TiO_2/Nb$  clearly distinguishes between the tholeitic and transitional Pololu series and the alkalic Hawi series. We then use the close relationships between  $TiO_2/Nb$  and the major elements in the fresh lavas (Spengler and Garcia, 1988) to estimate the composition of the parent material for each site (SI Fig. 1). The basaltic

parent material ensures the absence of ancient (radiocarbon-dead) sedimentary OC that would otherwise interfere with radiocarbon signatures of decaying plant material and heterotrophic biomass in the soil.

There is a steep precipitation gradient on the leeward side of Kohala mountain: annual precipitation increases from 25 mm to 4000 mm over 15 km map distance (Fig. 1). Our transect has a map distance of approximately 5 km, and the sites range in elevation from 1133 to 1554 m. We estimate precipitation from the Online Rainfall Atlas of Hawai'i (Giambelluca and Sanderson, 2013). The interaction of the forest canopy with fog and small droplets results in the collection of additional water, and total water input can be significantly greater than the rainfall model predicts (Chadwick et al., 2003; Marin-Spiotta et al., 2011; Kramer et al., 2012). At another forested site on the island of Hawai'i at a similar elevation (1190 m) the total water input (fog + rainfall) averaged 161% of rainfall alone for a six year period (Carillo et al., 2002). We do not have fog water measurements at our sites, but field observations over several years qualitatively indicate that the higher sites in our study area have substantially more fog. We therefore expect that the rainfall model underestimates the total water input, particularly at the higher elevations.

The precipitation gradient causes a systematic increase in water content and concomitant decrease in pH of the soil (Perez-Fodich and Derry, 2019). The changes in pH are driven by changes in the water content, base cation depletion, and organic acid input. Once water inputs routinely exceed potential evapotranspiration, pH drops below 6 and the weathering intensity increases sharply (Chadwick et al., 2003). This increase in weathering intensity alters the mineralogy of the soil, especially with respect to the content of iron minerals. Iron-bearing short range order (SRO) minerals, such as ferrihydrite and nanogoethite, are abundant in the lower portion of the precipitation gradient and then decrease as soils become increasingly saturated (Thompson et al., 2006b). In the wettest (high MAP) sites, the pH drops below 4 and is no longer buffered by base cations (Torn et al., 1997; Kramer et al., 2012), and soil minerals are dominated by imogolite and allophane (Chadwick et al., 2003). In all the sites across the gradient studied here there is strong depletion of base cations, with sufficiently low pH that carbonate precipitation does not occur. At the higher elevation sites there is extensive Fe loss resulting from reductive dissolution of Fe oxide phases (Thompson et al., 2006a; Thompson et al., 2006b; Buettner et al., 2014).

Across the 5 km transect, the vegetation changes from pasture to forest (Fig. 1 (inset)). The lower sites are located in pastureland and are currently protected by fencing for a restoration effort intended to rehabilitate the pre-contact native forest. In the early to mid 20th century the lower portion of Kohala was deforested and non-native Kikuyu grasses (*Pennisetum clandestinum*) were planted for cattle grazing. Grazing was stopped on this section of the mountain in the late 20th

 Table 1

 Characterization table for Pololu soils in this study.

Site Number	Site Designation	UTM Zone 5 Northing	UTM Zone 5 Easting	Elevation (m)	Estimated rainfall (mm)	Vegetation	# horizons collected	Sampled Depth (cm)
1	PL3717	213990	2220073	1133	1678	Pasture	6	79
2	PL3920	214196	2220432	1195	1784	Pasture	6	90
3	PL4169	214528	2220721	1271	1915	Pasture	7	105
4	PL4270	214653	222051	1301	2000	Pasture	5	90
5	PL4535	214971	2221596	1382	2107	Pasture	8	90
6	PL4625	214897	2221,40	1410	2154	Pasture	5	83
7	PL4697	215054	2221386	1432	2192	Pasture	8	93
8	PL4750	214,41	2221533	1448	2220	Pasture	7	97
9	PL4763	215050	2221442	1452	2226	Forest	7	95
11	PL4800	214737	2221190	1463	2246	Pasture	7	80
10	PL4782	215145	2221,88	1458	2236	Forest	7	65
12	PL4865	215230	2221617	1483	2280	Forest	5	60
13	PL4925	215332	2221715	1501	2311	Forest	5	60
14	PL4990	215379	2221798	1521	2345	Forest	6	67
15	PL5100	215471	2221975	1554	2403	Forest	4	61

century and active restoration began in the early 2000s. The Kikuyu grasses use the C4 photosynthetic pathway, while the forest is exclusively comprised of Oʻhia (*Metrosideros polymorpha*) and Hapuʻu pulu (tree fern: *Cibotium splendens*), which are C3. However, in the pasture soils, the  $\delta^{13}$ C signal of the C4 grasses does not extend below ~40 cm depth (Chadwick et al., 2007; Kelly et al., 1998).

Sampling sites were chosen on local areas of low slope with minimal signs of erosion or disturbance. We selected sites according to the distinct transitions in the soil properties which have been previously reported on the younger Hawi and Pololu lavas (Chadwick et al., 1999; Teutsch et al., 1999; Chadwick and Chorover, 2001) to test the changes in carbon persistence. These sites were chosen to extend over the redox transition zone, including soils that are periodically saturated and Fe depletion in the soils is important. There is significant color change from the drier sites, with bright orange/reddish soils to grey and mottled horizons in the upper MAP sites (Fig. 1).

At each of the 15 sites, an approximately 1 m soil pit was excavated for descriptive and collection purposes until reaching a restrictive layer or water table. Genetic soil horizons were collected resulting in 4–8 soil samples per site; in all we report data from 93 samples. All soil samples upon collection were refrigerated the same day and stored at 4  $^{\circ}\mathrm{C}$  until use. Soil samples were subsampled, freeze dried, and sieved to <2 mm. Any large and/or visible root material was removed from the sieved samples.

## 2.2. Inorganic geochemical methods

Dried samples were pulverized with an agate shatter box. Aliquots of samples were then combusted in a muffle furnace at 500 °C for 4 h and subsequently ignited at 950 °C for 30 min to remove all OC, structural water, and convert Fe<sup>2+</sup> to Fe<sup>3+</sup>. Ignited samples were fused with a 1:1 lithium metaborate to tetraborate flux mixture (Spex) with a flux:sample ratio of 4:1 at 1000 °C for 30 mins in a muffle furnace. Cooled glass beads were dissolved in a 10% HNO3/1% HF solution. Samples were immediately filtered through a 0.45 µm PTFE syringe filter and diluted by  $10\times$ . The samples were further diluted to  $10,000\times$  for analysis on a SpectroBlue ICP-OES (Ametek, Kleve, Germany) for major elements, and trace metals were analyzed on a Thermo Element II ICP-MS (Thermo Fisher Scientific, Waltham, MA). The USGS standard BHVO-2 was used as a reference material and procedural blanks measured every 10 samples. Quantification was achieved using matrix-matched intensity calibration curves derived from a set of USGS rock standards for both the ICP-OES and ICP-MS runs. Analytical uncertainties are within 5%, based on repeat analysis of standards and of selected samples. A subset of samples was duplicated beginning with the digestion step, and differences between duplicate preparations and analyses were <5% with a single exception (Table S6).

Element loss or gains are calculated relative to an "immobile" element (i), and normalized to the unweathered parent material (p). Kurtz et al. (2000) demonstrated that niobium (Nb) was well-suited as an index element in Hawaiian lavas, however due to the complex mixture of the Hawi and Pololu lava parent material at these sites, we use  $\text{TiO}_2$  as the index element (Vitousek and Chadwick, 2013). The lower inherent variability in parent material  $\text{TiO}_2$  than Nb, and in  $\text{Fe}_2\text{O}_3/\text{TiO}_2$ , makes normalization to  $\text{TiO}_2$  less sensitive to uncertainties in the parent material composition. The mass transfer coefficients,  $\tau_{ij}$ , are a measure of weathering where the abundance of a mobile element (j) in the weathered material (w) is compared to an immobile element (i):

$$\tau \tau_{ij} = \left(\frac{C_{i,p}}{C_{i,w}} \times \frac{C_{j,w}}{C_{j,p}}\right) - 1$$

## 2.3. Bulk organic matter analysis

For organic matter analysis, dried, ground samples were loaded into

tin capsules for combustion. No acid pretreatment was applied because these samples contain no carbonates. Total organic carbon (TOC), nitrogen (TN),  $\delta^{13}C$ , and  $\delta^{15}N$  were measured at the Cornell Stable Isotope Laboratory on a Thermo Delta V Advantage coupled EA-IRMS (Thermo Scientific, Waltham, MA, USA). Data is corrected following standard procedures;  $\delta^{13}C$  is reported relative to Vienna Pee Dee Belemnite (VPDB) and  $\delta^{15}N$  is reported relative to the  $^{15}N/^{14}N$  ratio in air. Bulk radiocarbon ( $^{14}C$ ) analysis was carried out at ETH-Zurich (see below). A subset of samples was repeated at both the NOSAMS and ETH radiocarbon facilities, and differences between duplicate preparations and analyses were  $\leq 5\%$  (SI Table 7).

## 2.4. Lipid extraction and isolation

Lipid biomarkers (n-alkanoic acids, FAs) were extracted from a subset of five soil profiles across the Kohala climate gradient (Table 2). Due to sample availability and abundance of extracted biomarkers, not every lipid fraction was extracted and measured for each sample. Lipids were extracted from soils using procedures outlined in (van der Voort et al., 2017). Briefly, ≈2 g of freeze-dried, ground soil was extracted in 9:1 dichloromethane:methanol (DCM:MeOH) by microwave extraction (1600 W, 100 °C, 20 min) (CEM MARS 6 microwave extraction system). Soil samples were rinsed 3 times in 9:1 DCM:MeOH and the total lipid extract (TLE) was dried at 30 °C under a low flow of N2. The TLE was saponified using 0.5 M KOH dissolved in MeOH for 2 h at 70 °C. NaCl was added to the cooled, saponified TLE and a neutral fraction was extracted (3x) with hexane (Hx). The remaining saponified TLE was adjusted to pH 2 using concentrated HCl, and an acid fraction was obtained by extraction with 4:1 Hx:DCM and then dried under N2. The acid fraction was methylated for 12 h at 70 °C using 95:5 MeOH:HCl. The resulting fatty acid methyl esters (FAMEs) were extracted (Hx; 3×) and dried under N<sub>2</sub>. The FAMEs were then cleaned using a 2% deactivated silica gel column (4 cm) with a layer of Na<sub>2</sub>SO<sub>4</sub> (to remove residual water), eluting with 4 ml Hx, 4 ml DCM:Hx (2:1), and 4 ml DCM.

The FAMEs were separated and quantified by gas chromatography flame-ionization detection (GC-FID) (Agilent Technologies 7890A, non-polar column HP5, 30 m  $\times$  0.32 mm i.d., 0.25  $\mu$ m film thickness). Biomarker concentrations were determined using an external calibration curve (Sigma Aldrich standards 1819-1 AMP C<sub>4</sub>-C<sub>24</sub> for FAMES). Individual compounds were separated by preparative capillary gas chromatography (PCGC) (Gerstel preparative fraction collector) (Eglinton et al., 1996). For this study we collected the fatty acid homologues C<sub>16</sub>, C<sub>18</sub>, C<sub>24</sub>, C<sub>26</sub>, C<sub>28</sub>, individually, and C<sub>30</sub> + C<sub>32</sub> collectively. PCGC traps were rinsed with 1 ml Hx:DCM (9:1) to recover the purified FAMEs. A subsample of the purified compound(s) was analyzed by GC-

**Table 2**Samples used for lipid biomarker extractions.

Site/ Sample Horizon	Depth (cm)	Bulk OC (%)	Bulk δ <sup>13</sup> C (‰)	Bulk <sup>14</sup> C Content (Fm)	Conventional <sup>14</sup> C Age (years)	Bulk Δ <sup>14</sup> C (‰)
PL4169-2	15–25	12.77	-18.81	1.00	modern	-7
PL4169-4	33-45	15.80	-24.66	0.68	3098	-325
PL4169-6	70-90	15.02	-25.80	0.29	9944	-712
PL4535-2	10-16	14.85	-24.51	0.50	5568	-503
PL4535-5	36-45	12.96	-25.12	0.41	7162	-593
PL4535_6	45-65	14.88	-25.17	0.30	9672	-702
PL4535-8	80-90	14.99	-24.98	0.23	11,806	-771
PL4800-2	8-15	6.14	-22.61	0.79	1894	-216
PL4800-4	25-40	5.76	-24.96	0.66	3338	-345
PL4800-5	40-50	10.26	-25.25	0.44	6595	-563
PL4800-7	65-80	12.25	-25.69	0.18	13,775	-821
PL4782-3	17-26	10.85	-26.23	0.96	328	-47
PL4782-5	36-46	11.51	-26.13	0.83	1497	-176
PL4782-7	55-65	14.12	-25.91	0.72	2639	-285
PL4925-2	10-17	31.03	-26.54	1.04	Modern	32
PL4925-3	17-30	7.57	-27.07	0.80	1793	-206
PL4925-5	45–60	8.11	-27.08	0.75	2311	-255

FID to check for yield and purity.

Separated individual compounds were cleaned over a 1 cm dry 1% deactivated silica gel column with 4 ml DCM into a combusted quartz tube and dried at 40 °C under minimal  $N_2$  flow. Vacuum sealed samples were combusted overnight at 850 °C with Ag-copper oxide (CuO) to ensure complete oxidization to CO<sub>2</sub>. CO<sub>2</sub> was cryogenically purified on a vacuum line and transferred to a Pyrex tube (63 mm  $\times$  4 mm o.d.) compatible with the gas interface system (GIS) (Wacker et al., 2010; McIntyre et al., 2017).

## 2.5. Biomarker carbon isotopic (13C and 14C) analysis

For radiocarbon analysis, freeze-dried, homogenized samples were loaded into tin capsules and analyzed using a coupled elemental analyzer-accelerator mass spectrometer (EA-AMS) MIniscale CArbon DAting System (MICADAS) instrument at the Laboratory for Ion Beam Physics (LIP) (ETH, Zurich, Switzerland) (Synal et al., 2007). Radiocarbon data are reported in 'fraction modern' (Fm) (Stuiver and Polach, 1977). Combusted CO<sub>2</sub> from the FAME samples were introduced directly as CO<sub>2</sub> into the AMS via a cracker inlet (Mcintyre et al., 2017). Resulting data for samples were blank corrected by isotope mass balance as described in Haghipour et al. (2019). For biomarker  $\delta^{13}$ C analysis, aliquots of silica gel-cleaned acid and non-polar fractions were measured in duplicate by gas chromatography-isotope ratio mass spectrometry (GC-IRMS) at ETH. Both the <sup>14</sup>C and <sup>13</sup>C FAME data were corrected for methyl carbon associated with derivatization. Error was propagated throughout all calculations according to Haghipour et al. (2019). All statistical analyses were performed with Matlab (version R20018b).

#### 3. Results

## 3.1. Iron oxide variability

There is a clear relationship between MAP and Fe content of the soils (Fig. 2). We found significant iron loss ( $\tau Fe_{Ti}$  values < -0.8) in soil profiles with precipitation above >2200 mm yr<sup>-1</sup>. Soils in the drier, lower elevation portion of the gradient have excess Fe, with  $\tau Fe_{Ti}$  values averaging 0.6–0.2, with a transition in Fe content starting at 2100 mm yr<sup>-1</sup>. This excess Fe is associated with local dust deposition from lower sites on the arid portion of the gradient not included in this study where grazing has denuded the original vegetation community (personal communication with O. Chadwick). Fe-rich dust can occasionally be observed over the lower portions of the gradient during dry conditions but is not observed or known to impact the higher elevation section of the gradient due to persistent trade winds and downslope air movement.

In the wettest sites (i.e., rainfall greater than 2200 mm/year) most of the Fe originally present in the rock is not retained in the soils. These soils are gleyed and visibly iron-depleted (Fig. 1), and  $\tau Fe_{Ti}$  values approach -0.9 to -1 (Fig. 2). We interpret the shift in TiO2/Nb to higher values in the deepest part of the profile (SI Fig. 1) to mark a transition from Hawi-derived material to Pololu derived material. In this particular site the deeper and older Pololu has undergone less weathering, or weathered material may have been removed prior to or coincident with deposition of the Hawi-derived material. There is one exception in the two deepest horizons at PL4990, where  $Fe_2O_3$  is measured at 27 and 28% ( $\tau Fe_{Ti} > 0$ ) (Fig. 2). In deepest horizons in the PL4990 site, TiO2/Nb shows influence of a geochemically distinct parent material with little alteration due to weathering, consistent with less chemical depletion overall. While PL4990 receives rainfall of >2200 mm/year, there is significant vertical variation in iron content at this site.

When Fe is depleted in the soils, the mineral matrix becomes a mixture of Al, Si, and Ti oxy-hydroxides (SI Table 2).  $Al_2O_3$  is always at least 14 wt% in the soil samples and can comprise nearly 70% of the mineral portion of the soil sample in some horizons. Al depletion is consistent with the presence of organic acids in the soils (Perez-Fodich and Derry, 2019). Si is generally substantially depleted. Si/Al ratios are

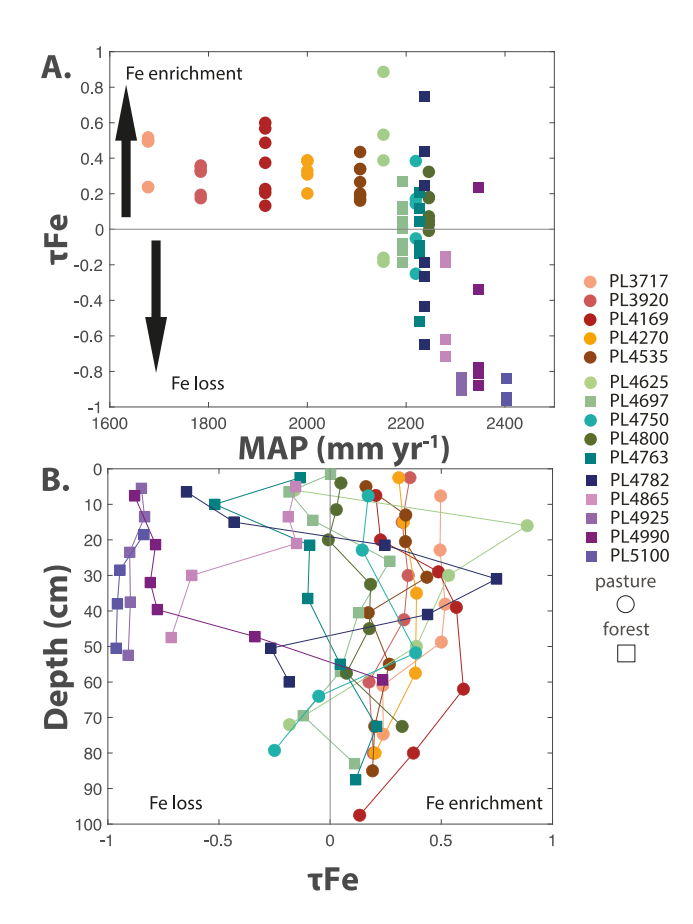


Fig. 2. A: Iron loss as measured by the normalized  $\tau Fe$  values across the MAP gradient. The extensive Fe loss occurs at precipitation values > 2200 mm yr $^{-1}$ . Fe loss ( $\tau_{Fe}$ ) across the gradient. B.  $\tau Fe$  depth profiles for each of the 15 sites. Tau values are normalized to TiO $_2$ . At sites with MAP > 2200 mm yr $^{-1}$  there is significant Fe loss, however in the drier part of the gradient, there is Fe enrichment (excess Fe), most likely derived from local dust deposition from very dry sites below our study site.

generally highest in the near-surface horizons, and in many cases exceed values for allophane (1.3–2.0), consistent with active recycling of biogenic silica in Hawaiian soils (Derry et al., 2005).

## 3.2. Bulk organic matter contents and characteristics

Generally, OC concentrations are highest in the surface horizons and decrease with depth (Fig. 3A). In the surface horizons of sites receiving between 1700 and 2000 mm yr $^{-1}$  MAP (all pasture sites), %OC ranges from 15 to 20% and decreases to 5–10% for the lowest elevation profiles (PL3717, PL3920, and PL4720). Above 2000 mm yr $^{-1}$  MAP, for the subset of pasture sites, surface soils have about 20% OC and then decrease to a constant value of 10–12% OC below 30 cm. The forest soil in the intermediate MAP range (PL4763) has surface soil horizons with 40 and 33% OC, while corresponding deeper soil horizons drop to 12% OC, similar to the pasture sites. In sites with MAP greater than 2200 mm yr $^{-1}$ , carbon concentrations are variable among profiles, but are generally higher, ranging from 10 to 45% OC in surface horizons and 5–27% in deeper horizons. We report C:N ratios and  $\delta^{15}$ N (%) values in the supplementary information (SI) (SI Figs. 2 and 3).

Stable carbon isotopic ( $\delta^{13}$ C) values of bulk SOC record the conversion from a forest utilizing the C3 photosynthetic pathway to a C4 pasture of introduced grasses along the lower half of the gradient (Fig. 3B). In the drier sites, surface soils and shallow mineral soils (<37 cm) record <sup>13</sup>C enrichment with  $\delta^{13}$ C values of -16 to -19%. Deeper in the soil profile (>37 cm),  $\delta^{13}$ C values are lower, averaging  $\sim -26$ %. The

K.E. Grant et al. Chemical Geology 587 (2022) 120629

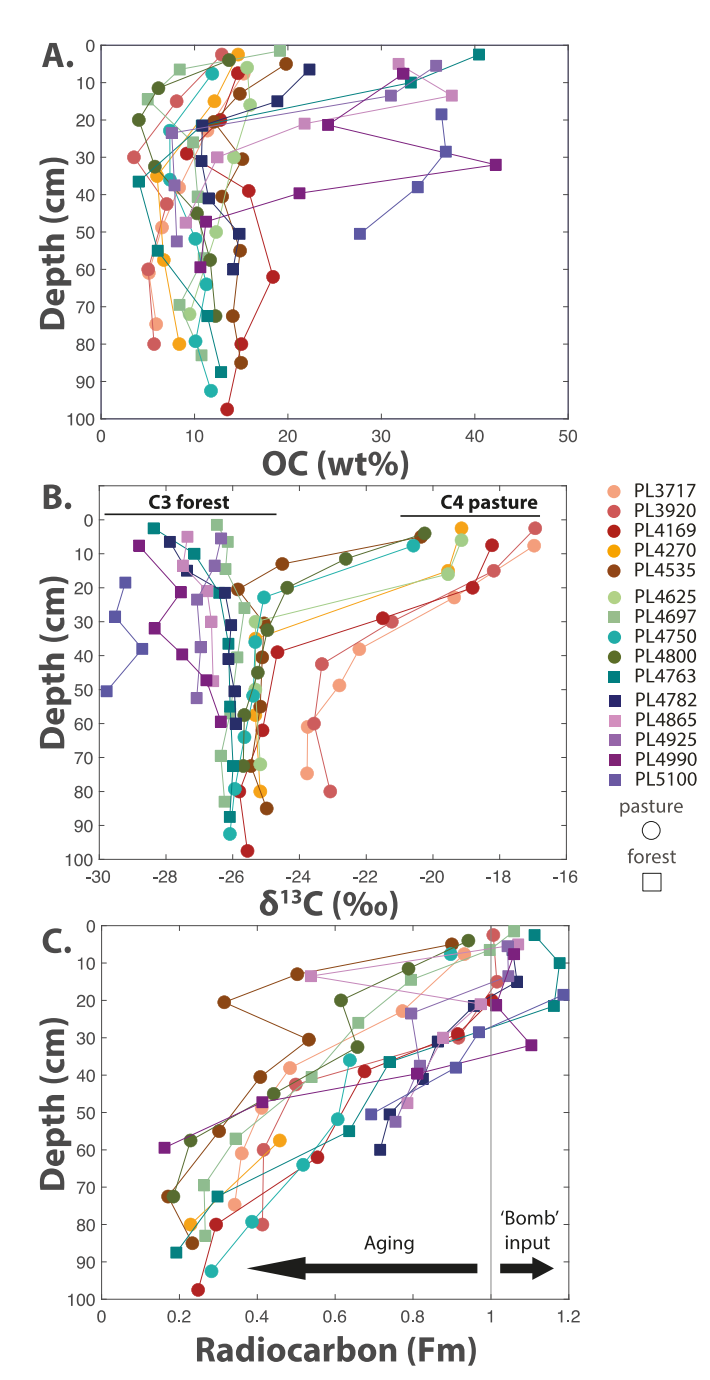


Fig. 3. Carbon concentration and isotope variation (%OC,  $\delta^{13}$ C, and Fm) with depth for the 15 soil profiles (13 for radiocarbon). Forest soils are represented by filled squares, and pasture sites have circle markers. Soil profiles range in MAP from 1.7 to 2.4 m  ${\rm yr}^{-1}$ . A: generally, %OC decreases by depth in each soil profile, however in some horizons OC can accumulate at depth. B. Surface soils of the drier, pasture sites have higher  $\delta^{13}$ C values (-16 to -20%) consistent with recent (20th century) C4 grass inputs, while subsurface soils, below 40 cm, show no influence from recent C4 vegetation (-23 to -25%). The surface soil  $\delta^{13}$ C values diverge between pasture sites ( $\sim -20$ %) and the forest site (-27%). At the highest MAP sites, in both the surface and subsurface soils,  $\delta^{13}$ C values are relatively invariant with depth (surface, -27%; deep -26%). The highest elevation site, PL5100, is one exception, where  $\delta^{13}\text{C}$  values are more depleted, -29%. C: For the 15 soil profiles, radiocarbon (14C) is presented by depth and reported in Fm. Across the gradient, Fm values in the surface horizons correspond to modern OC (Fm > 1) and decrease rapidly by depth to values of 0.23 to 0.4 (7000 to 12,000 <sup>14</sup>C years) in drier sites, and values at depth of 0.7–0.8 (<sup>14</sup>C age of 2000–3000 years). There is one exception, in the high MAP site PL4990 profile, where old ages (Fm of 0.41 and 0.16) are measured.

two driest sites have higher  $\delta^{13}\text{C}$  values at depth (-23%) compared to other deeper horizons in the low MAP zone. Above 2000 mm yr $^{-1}$ , an isotopic difference between pasture and forest sites is clearly evident until about 30 cm, with higher  $\delta^{13}\text{C}$  values (-20%) in pasture (C4) sites compared to forest (C3) sites (-26 to -27%). The isotopic signatures for these two different types of sites converge to  $\approx -26\%$  below 30 cm. When MAP exceeds 2300 mm yr $^{-1}$ ,  $\delta^{13}\text{C}$  values are largely invariant with depth, averaging around -27%. SOC  $\delta^{13}\text{C}$  values are as low as -29% at the highest site, PL5100, the most  $^{13}\text{C}$ -depleted value for bulk SOC obtained in the dataset.

Radiocarbon measurements (Fm) on bulk SOC samples were measured at 14 of the sites, with 83 total analyses. In general, OC ages increase (Fm decreases) with increasing soil depth (Fig. 3C). In the low MAP zone, surface soils have modern Fm values (Fm  $\sim$  1). There is heterogeneity within surface soil Fm values; with the first 20 cm in four of the dry sites recording a range of Fm values from 1.04 to 0.5. At depth, these dry sites contain strongly <sup>14</sup>C-depleted (older) carbon with Fm values of 0.2 to 0.4 (12,000 to  $7100^{-14}$ C years). In the intermediate MAP zone, surface horizons have Fm values of 1 or greater, decreasing to values of 0.28 to 0.18 in the deeper horizons (corresponding to <sup>14</sup>C ages of 10,160 to 13,580 yrs). The age trends are very similar between the different profiles, however, the higher elevation pasture site (PL4800) has older ages at each depth than a forest site at similar elevation (PL4763) (Fig. 3C). In the higher MAP sites, SOC in shallow soils is also close to modern, but SOC at depth is generally much younger than at the drier sites. With the exception of the two deepest horizons of the PL4990 site (Fm values of 0.41 and 0.16), and a shallow horizon of the PL4865 site (Fm value of 0.54), Fm values in the wet sites are never below 0.7 (i. e., older than 2800 <sup>14</sup>C years) (Fig. 3).

## 3.3. Biomarker concentrations

Lipid biomarkers varied in normalized concentration of extracted lipid ( $\mu$ g/gTOC) both between individual homologues and as a function of depth in a single profile. For the n-alkanoic acids (fatty acids, FA), three pasture soils (PL4169, PL4535, and PL4800) and two forest soils (PL4782 and PL4925) were analyzed (n=15) (SI Table 3). Generally, short-chain ( $C_{16}$  and  $C_{18}$ ) fatty acids (SCFAs) are more abundant in the shallower horizons and decrease with depth. While long-chain (i.e.,  $>C_{24}$ ) fatty acids (LCFAs) are less abundant in the deeper horizons (>30 cm), there is a difference between the forest and pasture sites, where LCFAs are more abundant in the forest sites.

## 3.4. $\delta^{13}C$ of n-alkanoic acids

From the 5 soil profiles, stable carbon isotope ratios ( $\delta^{13}$ C values) of the FAs were measured at multiple depths (Fig. 4). We compared this FAs  $\delta^{13}$ C signature to bulk SOC  $\delta^{13}$ C values. The  $\delta^{13}$ C values of the LCFAs were consistently lower than both the bulk and the SCFAs. Although more <sup>13</sup>C depleted than the bulk SOC or SCFAs from the same horizons, LCFAs from shallow depths (<20 cm) at two of three grasslands sites are shifted to more enriched values relative to LCFAs at depth, consistent with input of C4 grass-derived carbon. The LCFAs in deeper soils are  $^{13}$ C-depleted, with  $\delta^{13}$ C values ranging from -29 to -33% at all sites. At the pasture sites (PL4169, PL4535 and PL4800), SCFAs from the shallower horizons (< 40 cm) have higher  $\delta^{13}$ C values compared to the bulk SOC. The difference between bulk and SCFA  $\delta^{13}$ C values suggests that the bulk SOC at these depths retains a greater fraction of C3-derived carbon from prior to the land use conversion, while the SCFAs incorporate proportionally more C4-derived carbon. At depths  $\geq$ 40 cm, the  $\delta^{13}$ C values for SCFAs are lower than or equal to the bulk values at all sites but are still higher than the LCFAs.

## 3.5. Radiocarbon age of n-alkanoic acids (Fatty Acids)

Generally, <sup>14</sup>C ages of LCFAs are older than that of corresponding

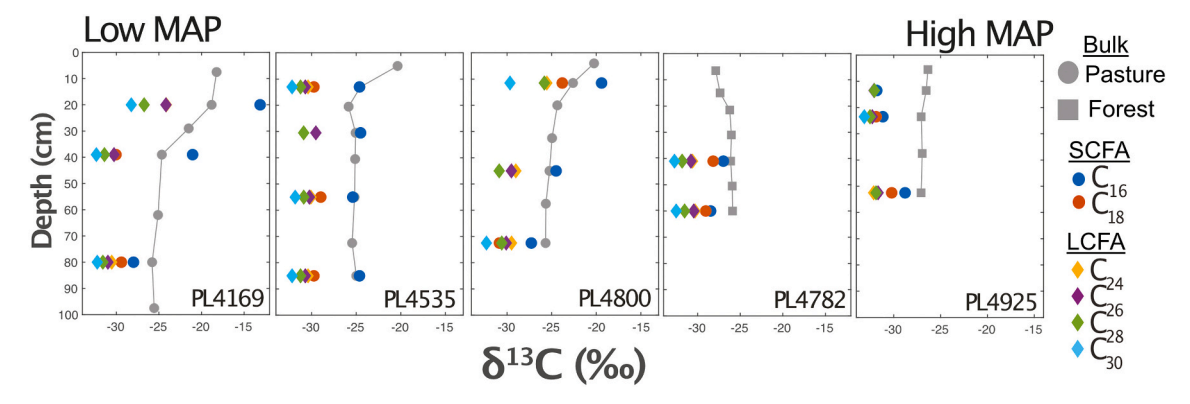


Fig. 4. Stable carbon isotopic variability in bulk OC and individual n-alkanoic (fatty) acids (FAs), expressed as  $\delta^{13}$ C (‰) for five soil profiles across pasture and forested Kohala gradient sites spanning a MAP of 1900 to 2300 mm/year. Each FA was measured in duplicate. Differences between replicates are smaller than the symbol sizes. Generally, long-chain (>C<sub>24</sub>) FAs (LCFAs)are depleted in  $^{13}$ C relative to the bulk and the SCFA. In much of the pasture,  $C_{16}$  has a much heavier  $\delta^{13}$ C signature than the LCFAs reflecting recent C4 grassland input into the soil. Error bars on the  $^{13}$ C isotope measurements are all smaller than the symbol.

bulk OC in each of the 5 soil profiles measured (Fig. 5).

This difference was most pronounced in the deeper soil horizons, whereas the shallow, near-surface horizons showed very similar bulk, LCFA, and SCFA values. The SCFA data we obtained is mostly from deeper horizons, where the SCFA ages are much younger than the bulk or LCFA values. The SCFAs, even in the deep soil horizons (>30 cm) were still near modern in the wetter sites ( $Fm \sim 0.9$ ;  $\sim 850^{14}$ Cyrs), while in the dry sites, SCFAs are significantly younger than corresponding bulk OC and LCFAs (Fm = 0.405 to Fm = 0.7;  $\sim 2800^{14}$ C yrs).

Bulk OC <sup>14</sup>C ages are much younger in sites where Fe is significantly depleted by reductive dissolution and the soil is gleyed (Fig. 6, Fig. 7). LCFA <sup>14</sup>C ages from these sites are also much younger than the LCFAs in the Fe-rich sites (Fig. 7). Specifically, when  $\tau$ Fe is > -0.5 and reactive Fe oxides are abundant, LCFAs are old (Fm of 0.1–0.2; ~18,000–12,000 <sup>14</sup>C yrs). There is a strong negative correlation between  $\tau$ Fe and the radiocarbon values of LCFAs in the deep soil ( $r^2 = 0.9$ , p < 0.05), this trend is also seen between  $\tau$ Fe and the topsoil LCFAs, but the slope is shallower and the correlation much weaker ( $r^2 = 0.27$ , p < 0.5) (Fig. 8).

## 4. Discussion

## 4.1. Carbon is destabilized in Fe reducing zones

We find consistently younger OC at the higher MAP sites which experience episodic saturation, influenced in part by local microtopography. The development of gleyed soils with substantial Fe loss at

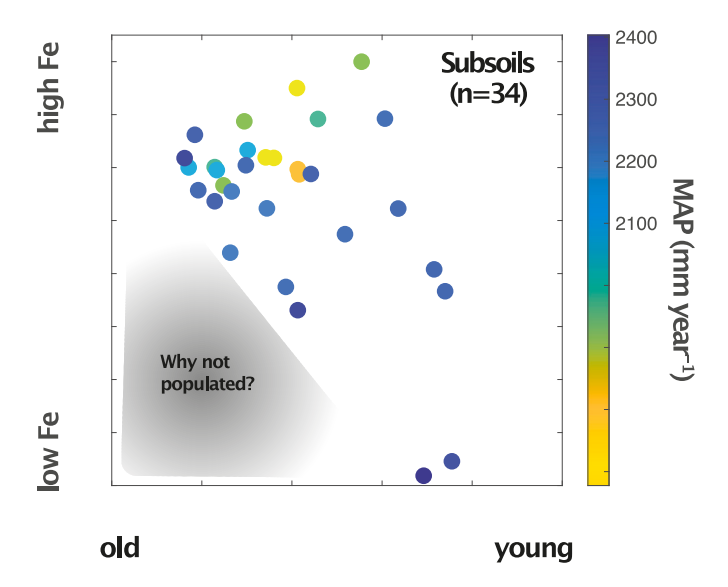


Fig. 6. Bulk radiocarbon (Fm) values correlated with normalized Fe loss ( $\tau$ Fe) in subsoils >37 cm. The color coding indicates MAP across the gradient. While we see a range of radiocarbon ages at relatively high Fe contents, no "old" carbon is observed when  $\tau$ Fe is <-0.4.

similar Hawaiian sites has been shown to be related to episodic

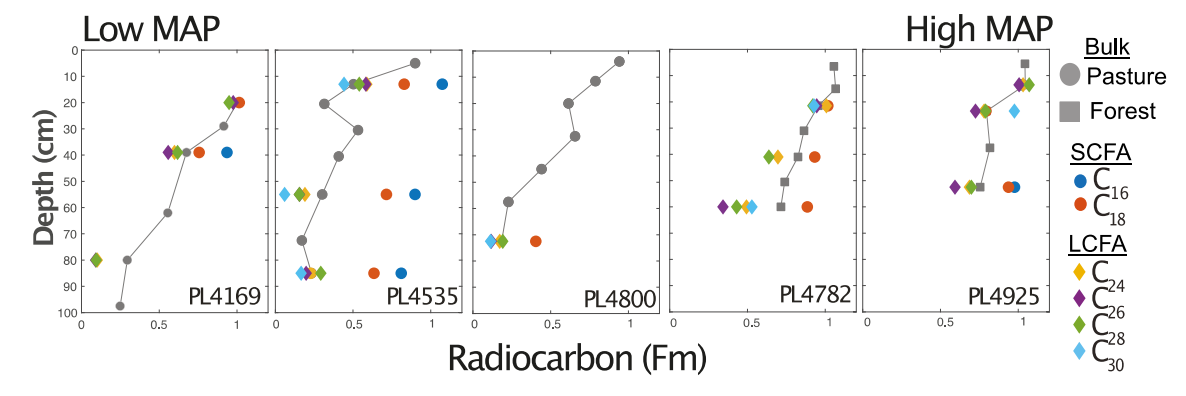


Fig. 5.  $^{14}$ C variability in bulk OC and individual n-alkanoic (fatty) acids (FAs), expressed as Fm for five soil profiles across pasture and forested Kohala gradient sites spanning a MAP gradient of 1900 to 2300 mm/year. Differences between replicates are smaller than the symbol sizes. Generally, in surface horizons, FAs (all homologues) had radiocarbon signatures that were not significantly different than the bulk values. Deeper in the profiles, there is greater spread in radiocarbon values. Generally, the LCFAs are older than the bulk soil samples. In all deep sites SCFAs ( $C_{16}$  and  $C_{18}$ ) are younger than the LCFAs and the bulk sample. Error bars on the radiocarbon measurements are all smaller than the symbol.

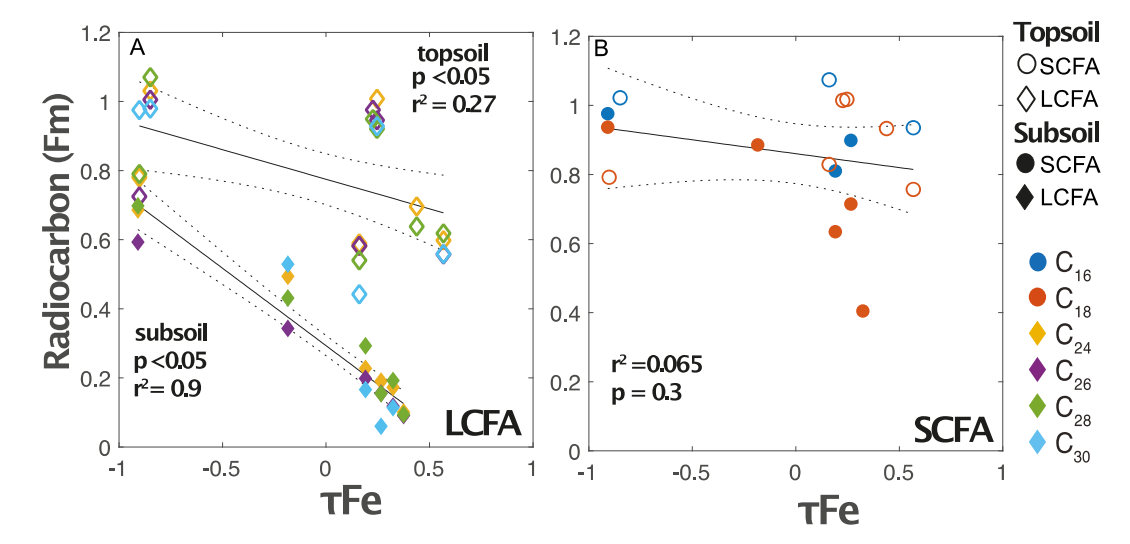


Fig. 7. A: Correlations between normalized Fe loss ( $\tau$ Fe) and radiocarbon (Fm) between the long chain fatty acids (LCFAs) ( $C_{24}$ - $C_{30}$ ) in the top soil (<37 cm) and subsoils (>37 cm). There is a strong negative correlation between the LCFAs and  $\tau$ Fe in the subsoils, this negative trend is seen to a lesser extent in the topsoil. This trend suggests that LCFA persistence is due to the presence of Fe oxides in the less weathered soils. B: The SCFA are younger and have no correlation between Fe and age, suggesting soil microbes assimilate younger carbon in all sites. Analytical error bars on the radiocarbon measurements are all smaller than the marker. Dashed lines indicate 95% C.I. on the linear regressions.

saturation and oxygen deficient conditions (Thompson et al., 2006a, 2006b; Thompson et al., 2011). Under such conditions SOC decomposition is restricted by oxygen availability, with oxygen limitation leading to high SOC concentrations, long SOC turnover times and old <sup>14</sup>C ages. Indeed, the highest SOC concentrations observed along our transect are found in the high MAP gleyed sites, with up to 45 wt% OC. However, most of the higher MAP sites in fact have young OC 14C ages, and their ages are clearly related to Fe loss (Fig. 6). Notably, 14C ages are substantially younger at the Fe-depleted sites than nearby sites that retain Fe (Fig. 2b). Furthermore, in sites where Fe is lost, we did not find <sup>14</sup>C activity below Fm values of 0.7 (or  $\sim 2800^{14}$ C yrs). In Fig. 6, there is a region (highlighted in grey) where we would expect older ages of accumulating OC due to increases in saturation, but we do not find bulk <sup>14</sup>C older than 2800 years in Fe-depleted samples from wet sites. The correspondence of the individual lipid ages and bulk ages suggests the apparent lack of 'old OC' from wetter sites is not related to an increased input of younger OC diluting the older SOC pool. Indeed, if that were the case, we would expect to find similarly aged LCFAs at the wet and dry sites, which is not the case. We did not find any 'old' LCFA values in any samples with extensive Fe loss (Fig. 7).

With the loss of Fe SRO mineral surfaces, OC stabilization is likely to shift from Fe-mediated interactions to other mineralogical or environmental controls (Kleber et al., 2007). It was recently reported that the continued persistence of OC in Fe depleted soils might be associated with the soil aluminum phases (Possinger et al., 2020; Inagaki et al., 2020). However, in our study the remaining mineral matrix consists primarily of Si, Al, and Ti as SRO minerals (SI Table 3), yet the age of OC is younger in these samples. Despite the presence of potentially reactive surfaces in the Fe-depleted material, all measured carbon fractions are young, leading us to hypothesize that Fe-mineral stabilization is the main driver of mineral-associated OC persistence in this setting. Consequently our data set is most consistent with Hypothesis 2, that the presence of SRO phases, especially Fe bearing ones, is the main control on the abundance of old SOC.

The removal of reactive Fe SRO mineral surfaces has been shown to release OC in a laboratory setting (Pan et al., 2016). Based on thermodynamics of reducing environments, when soils are saturated,  $O_2$  is depleted and anoxic respiration slows organic matter decay (Greenwood, 1961; Lovley and Phillips, 1986). In these conditions, instead of  $O_2$ , the less energetically favorable electron acceptor Fe(III) is utilized

for OC respiration (Dubinsky et al., 2010). This is evident in the gleyed or mottled soil, where bright red SRO Fe minerals are interspersed with completely Fe depleted zones (Fig. 1). The removal of Fe oxide phases from Hawaiian soils is thought to be aided by enhanced colloidal transport and Fe<sup>2+</sup> leaching (Buettner et al., 2014; Henderson et al., 2012; Thompson et al., 2008, 2006a, 2011). There is emerging evidence from laboratory simulation experiments under oscillating redox conditions that reduced Fe may directly enhance OC mineralization (Chen et al., 2020). These authors found that stable oxic conditions were required for Fe oxide protection of OC. We mostly found much younger ages (Fm = 0.7 vs Fm = 0.2) in these frequently saturated, intermittently reducing environments (Fig. 6), suggesting that OC is rapidly turning over with loss of Fe oxides, despite potential oxygen limitation on OC mineralization rates.

#### 4.2. Loss of 'old' previously stabilized OC

In the high MAP sites, there is some question about the historical presence of SRO Fe oxides (Torn et al., 1997). Specifically, was there ever 'old' mineral-stabilized OC at these sites? The answer to this question influences whether our observations reflect an inability for OC to persist to >2500 <sup>14</sup>C years at these sites or reflect a loss of previously stabilized old ( $> 2500^{-14}$ C years) OC from the system. On Kohala, evidence suggests that the second scenario is more plausible. The distribution of gleyed soils is patchy within the "high" MAP zone. Gleyed soils are found in areas of low topographic gradient, whereas adjacent steeper zones are visibly better drained and retain ferric iron. In the PL4990 (forest) site, well within the climate zone where we generally observe substantial Fe loss, iron remains locally abundant ( $\tau Fe_{Ti} > -0.5$ ) (Fig. 7). We found three horizons at this site that have old carbon (ca. 7000-14,000 yrs); all three have higher Fe retention than the surrounding horizons, with  $\tau_{Fe}$  values above -0.5. Fm values range from 0.41 to 0.16 (ca. 7100 up to 14,600 radiocarbon years), including the oldest sample in the entire dataset. Thus, adjacent sites with differences in local topography and iron loss have substantially different <sup>14</sup>C abundances, implying that it is iron and carbon loss rather than an inability to sequester carbon which is responsible for the observed Fe-<sup>14</sup>C correlation. Heterogeneity in iron distribution both within a single soil profile and between nearby sites is consistent with relatively recent development of Fe and old C loss rather than an inherited

characteristic from early phases of pedogenesis. However, irrespective of time scale of development, it is evident that the presence of Fe is necessary to retain OC for more than 14,000  $^{14}\mathrm{C}$  years in these basaltic andisols.

The study area is partially dissected by a developing stream network. The channel network is incising into the study area; however, the rate of propagation is unknown. Local channel relief is up to 6-9 m, although most is significantly less. One possibility is that post-glacial climate change has increased precipitation input into the study area, enhancing incision while at the same time driving low gradient sites to increasing saturation frequency. Evidence suggest an increase in MAP in Hawaii between the last glacial maximum (LGM) and present of at least a factor of two (Hotchkiss et al., 2000), more than sufficient to place our study site well below the precipitation threshold observed to drive substantial Fe loss during the LGM. As a preliminary working hypothesis, we thus propose that the high MAP sites where we now measure loss of both Fe and old carbon were drier, Fe-replete and had old carbon prior to the Holocene. We posit that the current absence of old SOC resulted from increased Holocene precipitation, redox destabilization of Fe(III) binding sites and the consequent mineralization of the old SOC. This is consistent with the findings in Hein et al. (2020), where since the LGM increased precipitation in the tropical Ganges-Brahmaputra basin led to an increase in the pace of soil carbon turnover (faster cycling = younger ages) and as a result a decrease in soil carbon stocks. The hydrological environment could be a key overall mechanism controlling OC persistence across the tropics and broadly more humid conditions since the LGM may have contributed to an increasing flux of CO2 from tropical

The difference we observe in age between SCFA and LCFAs is seen in other soils. van der Voort et al. (2017) found that SCFAs were younger and turned over more rapidly than the plant wax-derived LCFA, especially in deeper soil horizons, in two different alpine mountain soils. The SCFAs are non-specific lipids derived from multiple sources, such as microbes, plants leaves, and root biomass. They tend to be degraded more rapidly compared to LCFAs in many different environments (French et al., 2018). In deeper soils, SCFAs most likely originate from microbial communities consuming younger, translocated carbon such as DOC (van der Voort et al., 2019) or root exudates (Angst et al., 2016). We attribute the relatively young SCFA 14C signatures, compared to LCFAs in all measured horizons, as reflecting the influence of microbes preferentially mineralizing younger carbon and assimilation into microbial biomass. In contrast, the LCFAs are exclusively derived from plant wax lipids. The concurrence of young ages for bulk samples, SCFAs, and LCFAs for high MAP sites implies that the young ages for the former are not simply the result of dilution with younger carbon but must reflect loss of old carbon and broadly similar turnover rates of the different pools of carbon. Dilution of old carbon by a more abundant younger source is unlikely given that a study separating OC by thermal fractionation (ramped pyrolysis/oxidation; RPO) in a similar environment with relatively extensive Fe loss ( $\tau Fe_{Ti} = -0.5$ ) found no evidence of a significantly older OC component (Grant et al., 2019). In this study, the bulk OC <sup>14</sup>C age of the deepest horizon was only ~2500 years old (Fm, 0.75) and had relatively flat <sup>14</sup>C age distributions (only a 626 year difference among thermal fractions) implying the absence of any significantly older stabilized OC pool. This RPO-based finding is confirmed through direct molecular evidence in this current study as the LCFAs, the oldest component of the SOC, are younger in the low Fe soils and older in the more Fe rich soil and closely track the bulk 14C dynamics.

## 4.3. What carbon is most persistent?

During the 20th century, the forest was cleared and non-native pasture grasses were planted for grazing purposes in portions of the study area. Previous studies have reported this vegetation shift and its effect on below ground SOC storage are reflected in changes of  $\delta^{13}$ C

values down the soil profile. The land use change from pasture to forest does not appear to influence C composition or age in the bulk measurements of deep horizons at this site (Chadwick et al., 2007; Kelly et al., 1998). The conversion from pasture to forest is detectable in stable carbon isotopic signatures of both LCFAs and SCFAs from the shallow soil horizons. This conversion is also evident in the C<sub>16</sub> FAs (and to some extent  $C_{18}$ ) in surface samples from the higher elevation pasture sites PL4169 and PL4535. Specifically, the higher  $\delta^{13}$ C values of C<sub>16</sub> FAs suggest OC below ground has inherited the <sup>13</sup>C-enriched signature of C4 grasses; this could reflect microbial biomass or root input. Deeper downprofile, the <sup>13</sup>C-enriched grassland signature is no longer detected. The  $C_{16}$  FAs from shallow horizons at the pasture sites have higher  $\delta^{13}C$ values than the bulk SOC, implying that the vegetation change is reflected less rapidly in the bulk C than in the microbially-derived C<sub>16</sub> lipids. In the deeper horizons at all sites,  $\delta^{13}$ C values generally decrease with increasing chain length for all FAs.

Radiocarbon ages for the LCFAs are mostly older than the corresponding bulk ages, implying that these are among the most stable compounds in the soil. This observation is consistent with a study of LCFA ages in forested Swiss alpine soils (van der Voort et al., 2017; Gies et al., 2020). We find the oldest plant wax lipids deep in the soil profile, while C<sub>16</sub> and C<sub>18</sub> FAs are nearly always noticeably younger. The strong relationship between Fe loss and both bulk and LCFA ages in the soil suggests that Fe-SOC interactions play an important role in stabilizing SOC for long time scales. The young SCFA ages at depth are consistent with previous work that has demonstrated the transport of young carbon down-profile along preferential paths and deposition along cracks and ped surfaces in similar nearby soils (Marin-Spiotta et al., 2011). We hypothesize that the SCFAs found at depth are largely derived from the uptake of young carbon sources (e.g., DOC transported from upper soil horizons) by active microbial communities, such as proposed by van der Voort et al. (2019).

However, it is likely some input of root biomass contributes to the belowground OC. Increase in root biomass at depth would increase Fm values and shift  $\delta^{13}$ C values closer to the modern plant signatures (heavier in the pasture and closer to -27% in the forest). Roots generally have higher concentrations of C<sub>16</sub> and C<sub>18</sub> than higher order lipids (LCFAs) and with faster turnover could contribute to more stable SOC pools (Adamczyk et al., 2019). In a previous study of similar Hawaiian soils using thermal fractionation, there was no evidence of 'modern' "free" OC transported to deep horizons (Grant et al., 2019). A "DOClike" mineral-unassociated signature (Hemingway et al., 2019) was measured in the extremely organic rich Oa horizon, but not in deeper horizons (Grant et al., 2019). In a previous publication, we argue that in deeper horizons this transported OC is either adsorbed to the soil mineral surface and/or assimilated into microbial biomass, resulting in an alteration of its activation energy. This result could be explained by an increase in root biomass at depth. Because <sup>14</sup>C abundances in the deep soils are quite low, this effect is more visible in the <sup>14</sup>C content than in the  $\delta^{13}$ C signature, even under the pasture grasses. Yet, in some sites FA concentrations increase at depth, potentially pointing to in situ microbial activity (SI Fig. 2).

## 5. Conclusions

Soil profiles sampled across the precipitation gradient reveal a systematic increase in the  $^{14}$ C age of both bulk SOC and individual FAs with depth and a systematic decrease in age associated with increased precipitiation. This correspondence between the bulk and LCFA indicates that environmental factors - not intristic reactivity - controls the SOC age in the gradient. The short-chain ( $C_{16}$ ,  $C_{18}$ ) FAs are younger than the longer-chain plant-wax derived FAs for all soil profiles and all soil depths. These isotopic patterns are consistent with microbial incorporation of relatively recently synthesized carbon into short chain FAs, possibly transported down the soil column in cracks and along ped surfaces (Marin-Spiotta et al., 2011). Bulk SOC and LCFAs at depth show

K.E. Grant et al. Chemical Geology 587 (2022) 120629

no resolvable C4 contribution and older <sup>14</sup>C ages, indicating that these pools turnover more slowly. LCFAs are systematically older than the bulk and SCFAs in all profiles, suggesting that bulk SOC in deeper soils is comprised of both microbial products derived from younger substrates and older, plant-derived compounds.

There is significant Fe loss at higher MAP sites associated with episodic soil saturation and reductive Fe loss. The high MAP sites have higher OC contents, consistent with the expectation that saturated conditions should promote SOC storage. However, at these high MAP sites iron depletion is associated with much younger <sup>14</sup>C ages, in both bulk SOC and LCFAs, than at equivalent sample depths in sites that retain most Fe (2900 vs 14,200 <sup>14</sup>C years). The strong relationship between Fe loss and loss of old C is consistent with a Fe-C mineral stabilization mechanism for old C in the drier, Fe-rich sites. Based on field relations and persistence of old C in wet sites that retain Fe, we hypothesize that old OC was present at depth at all sites, but increased precipitation accompanying Holocene climate change pushed the higher elevation sites over a redox threshold, enhancing Fe loss. This Fe loss in turn destroyed Fe-C complexes, resulting in loss of previously stabilized carbon.

Climatically forced destabilization of Fe-C complexes has wide implications, as iron oxide phases are abundant and can interact with OC in many soil environments. 'Old' carbon in this and similar systems may thus be vulnerable to destabilization via climate change. Changes in climate that pushes soils to increasing water saturation, even episodically, may – despite slower decomposition under oxygen-depauperate conditions - increase the mobility and bioavailability of old, previously stabilized C, resulting in loss from the soil reservoir. This old carbon may not be replenished on a time scale meaningful to slow anthropogenic climate change and therefore represents a new source of  $\mathrm{CO}_2$  to the atmosphere, while decreasing the size of the soil OC reservoir.

## **Funding sources**

This work was partially supported by the Cornell University Atkinson Center Small Grant program. KEG was supported by the Cross-Scale Biogeochemistry and Climate – National Science Foundation Integrative Graduate Education and Research Traineeship grant# DGE-1069193 the Cornell Graduate Fellowship and NSF 1660923. L. Derry acknowldges support from the French Programmes d'Investissement de l'avenir, ANR-17-MPGA-0009 and NSF 1660923.

## **Declaration of Competing Interest**

The authors declare that they have no known competing financial interests or personal relationships that could have appeared to influence the work reported in this paper.

## Acknowledgements

We would like to thank Daniel Montluçon for his generous laboratory help and guidance, K. Grant would like to thank Gregg McElwee for assistance with ICP instrumentation at Cornell. Oliver Chadwick provided many very helpful conversations, in the field and lab, during all stages of this project.

## Appendix A. Supplementary data

Supplementary data to this article can be found online at https://doi.org/10.1016/j.chemgeo.2021.120629.

## References

Adamczyk, B., Sietiö, O.-M., Straková, P., Prommer, J., Wild, B., Hagner, M., Pihlatie, M., Fritze, H., Richter, A., Heinonsalo, J., 2019. Plant roots increase both decomposition and stable organic matter formation in boreal forest soil. Nat. Commun. 10, 3982. Angst, G., John, S., Mueller, C.W., Kögel-Knabner, I., Rethemeyer, J., 2016. Tracing the sources and spatial distribution of organic carbon in subsoils using a multibiomarker approach. Sci. Rep. 6, 29478.

- Beer, C., Reichstein, M., Tomelleri, E., Ciais, P., Jung, M., Carvalhais, N., Rödenbeck, C., Arain, M.A., Baldocchi, D., Bonan, G.B., Bondeau, A., Cescatti, A., Lasslop, G., Lindroth, A., Lomas, M., Luyssaert, S., Margolis, H., Oleson, K.W., Roupsard, O., Veenendaal, E., Viovy, N., Williams, C., Woodward, F.I., Papale, D., 2010. Terrestrial gross carbon dioxide uptake: global distribution and covariation with climate. Science 329, 834–838.
- Buettner, S.W., Kramer, M.G., Chadwick, O.A., Thompson, A., 2014. Mobilization of colloidal carbon during iron reduction in basaltic soils. Geoderma 221–222, 139–145
- Bullen, T., Chadwick, O., 2016. Ca, Sr and Ba stable isotopes reveal the fate of soil nutrients along a tropical climosequence in Hawaii. In: Chemical Geology, 422. Elsevier B.V., pp. 25–45
- Carillo, J.H., Hastings, M.G., Sigman, D.M., Huebert, B.J., 2002. Atmospheric deposition of inorganic and organic nitrogen and base cations in Hawaii. Glob. Biogeochem. Cycles 16 (4), 1076.
- Chadwick, O.A., Chorover, J., 2001. The chemistry of pedogenic thresholds. Geoderma
- Chadwick, O.A., Derry, L.A., Vitousek, P.M., Huebert, B.J., Hedin, L.O., 1999. Changing sources of nutrients during four million years of ecosystem development. Nature 397, 491–497.
- Chadwick, O.A., Gavenda, R.T., Kelly, E.F., Ziegler, K., Olson, C.G., Elliott, W.C., Hendricks, D.M., 2003. The impact of climate on the biogeochemical functioning of volcanic soils. Chem. Geol. 202, 195–223.
- Chadwick, O.A., Kelly, E.F., Hotchkiss, S.C., Vitousek, P.M., 2007. Precontact vegetation and soil nutrient status in the shadow of Kohala Volcano, Hawaii. Geomorphology 89, 70–83
- Chen, C., Hall, S.J., Coward, E., Thompson, A., 2020. Iron-mediated organic matter decomposition in humid soils can counteract protection. Nat. Commun. 11, 2255.
- Coward, E.K., Thompson, A.T., Plante, A.F., 2017. Iron-mediated mineralogical control of organic matter accumulation in tropical soils. Geoderma 306, 206–2016.
- Dahlgren, R.A., Saigusa, M., Ugolini, F.C., 2004. The nature, properties and management of volcanic soils. Adv. Agron. 82, 113–182.
- Davidson, E.A., Janssens, I.A., 2006. Temperature sensitivity of soil carbon decomposition and feedbacks to climate change. Nature 440, 165–173.
- Derry, L.A., Kurtz, A.C., Ziegler, K., Chadwick, O.A., 2005. Biological control of terrestrial silica cycling and export fluxes to watersheds. Nature 433, 728–731.
- Dubinsky, E.A., Silver, W.L., Firestone, M.K., 2010. Tropical forest soil microbial
- communities couple iron and carbon biogeochemistry. Ecology 91, 2604–2612. Eglinton, T.I., Aluwihare, L.I., Bauer, J.E., Druffel, E.R.M., McNichol, A.P., 1996. Gas chromatographic isolation of individual compounds from complex matrices for radiocarbon dating. Anal. Chem. 68, 904–912.
- Eglinton, T.I., Galy, V.V., Hemingway, J.D., et al., 2021. Climate control on terrestrail biospheric carbon turnover. PNAS 118, e2011585118.
- Feng, X., Thompson, S.E., Woods, R., Porporato, A., 2019. Quantifying asynchronicity of precipitation and potential evapotranspiration in mediterranean climates. Geophys. Res. Lett. 46, 14692–14701.
- French, K.L., Hein, C.J., Haghipour, N., Wacker, L., Kudrass, H.R., Eglinton, T.I., Galy, V., 2018. Millennial soil retention of terrestrial organic matter deposited in the Bengal Fan. Sci. Rep. 8, 11997.
- Giambelluca, T., Sanderson, M., 2013. The water balance and climate classification. In: Sanderson, M. (Ed.), Prevailing Trade Winds: Weather and Climate in Hawai'i. University of Hawaii Press, Honolulu, p. 126.
- Gies, H., Hagedorn, F., Lupker, M., Montluçon, D., Haghipour, N., van der Voort, T.S., Eglinton, T.I., 2020. Millennial-age glycerol dialkyl glycerol tetraethers (GDGTs) in forested mineral soils: <sup>14</sup>C-based evidence for stabilization of microbial necromass. Biogeosciences 18, 189–205.
- Grant, K.E., Galy, V., V and Chadwick O. A., 2019. Thermal oxidation of carbon in organic matter rich volcanic soils: insights into SOC age differentiation and mineral stablization. Biogeochemistry 144, 291–304.
- Greenwood, D.J., 1961. The effect of oxygen concentration on the decomposition of organic materials in soil. Plant Soil 14, 360–376.
- Haghipour, N., Ausin, B., Usman, M.O., Ishikawa, N., Wacker, L., Welte, C., Ueda, K., Eglinton, T.I., 2019. Compound-specific radiocarbon analysis by elemental analyzeraccelerator mass spectrometry: precision and limitations. Anal. Chem. 91, 2042–2049.
- Hartmann, Jens, Durr, Hans, Moosdorf, Nils, Meybeck, Michel, Kempe, Stephan, 2012. The geochemical composition of the terrestrial surface (without soils) and comparison with the upper continental crust. Int. J. Earth Sci. 101, 365–376.
- He, Y., et al., 2016. Radiocarbon constraints imply reduced carbon uptake by soils during the 21st century. Science 353 (6306), 1419–1424. https://doi.org/10.1126/science.aad4273.
- Hein, C.J., Usman, M., Eglinton, T.I., Haghipour, N., Galy, V.V., 2020. Millennial-scale hydroclimate control of tropical soil carbon storage. Nature 581, 63–66.
- Hemingway, J.D., Rothman, D.H., Grant, K.E., Rosengard, S.Z., Eglinton, T.I., Derry, L.A., Galy, V.V., 2019. Mineral protection regulates long-term global preservation of natural organic carbon. Nature 570, 228–231.
- Henderson, R., Kabengi, N., Mantripragada, N., Cabrera, M., Hassan, S., Thompson, A., 2012. Anoxia-induced release of colloid- and nanoparticle-bound phosphorus in grassland soils. Environ. Sci. Technol. 46, 11727–11734.
- Hotchkiss, S., Vitousek, P.M., Chadwick, O.A., Price, J., 2000. Climate cycles, geomorphological change, and the interpretation of soil and ecosystem development. Ecosystems 3, 522–533.

K.E. Grant et al. Chemical Geology 587 (2022) 120629

- Huang, W.J., Hall, S.J., 2017. Elevated moisture stimulates carbon loss from mineral soils by releasing protected organic matter. Nat. Commun. 8.
- Inagaki, T.M., Possinger, A.R., Grant, K.E., Schweizer, S.A., Mueller, C.W., Derry, L.A., Lehmann, J., Kögel-Knabner, I., 2020. Subsoil organo-mineral associations under contrasting climate conditions. Geochim. Cosmochim. Acta 270, 244–263.
- Jackson, R.B., Lajtha, K., Crow, S.E., Hugelius, G., Kramer, M.G., Piñeiro, G., 2017. The ecology of soil carbon: pools, vulnerabilities, and biotic and abiotic controls. Annu. Rev. Ecol. Evol. Syst. 48, 419–445.
- Jenkinson, D.S., Rayner, J.H., 1977. The turnover of soil organic matter in some of the Rothamsted classical experiments. Soil Sci. 125, 298–305.
- Kaiser, K., Guggenberger, G., 2000. The role of DOM sorption to mineral surfaces in the preservation of organic matter in soils. Org. Geochem. 31, 711–725.
- Kelly, E.F., Chadwick, O.A., Hilinski, T.E., 1998. The effect of plants on mineral weathering. Biogeochemistry 42, 21–53.
- Kleber, M., Sollins, P., Sutton, R., 2007. A conceptual model of organo-mineral interactions in soils: self-assembly of organic molecular fragments into zonal structures on mineral surfaces. Biogeochemistry 85, 9–24.
- Kramer, M.G., Sanderman, J., Chadwick, O.A., Chorover, J., Vitousek, P.M., 2012. Long-term carbon storage through retention of dissolved aromatic acids by reactive particles in soil. Glob. Chang. Biol. 18, 2594–2605.
- Kurtz, A.C., Derry, L.A., Chadwick, O.A., Alfano, M.J., 2000. Refractory element mobility in volcanic soils. Geology 28, 683–686.
- Lehmann, J., Kleber, M., 2015. The contentious nature of soil organic matter. Nature 528, 60-68.
- Loh, et al., 2014. Variable ageing and storage of dissolved organic components in the open ocean. Nature 430, 877–881.
- Lovley, D.R., Phillips, E.J.P., 1986. Organic-matter mineralization with reduction of ferric iron in anaerobic sediments. Appl. Environ. Microbiol. 51, 683–689.
- Lutzow, M.V., Kogel-Knabner, I., Ekschmitt, K., Matzner, E., Guggenberger, G., Marschner, B., Flessa, H., 2006. Stabilization of organic matter in temperate soils: mechanisms and their relevance under different soil conditions - a review. Eur. J. Soil Sci. 57, 426–445.
- Marin-Spiotta, E., Chadwick, O.A., Kramer, M., Carbone, M.S., 2011. Carbon delivery to deep mineral horizons in Hawaiian rain forest soils. J. Geophys. Res. 116, G03011.
- McIntyre, C.P., Wacker, L., Haghipour, N., Blattmann, T.M., Fahrni, S., Usman, M., Eglinton, T.I., Synal, H.A., 2017. Online c-13 and c-14 gas measurements by ea-irmsams at eth zurich. Radiocarbon 59, 893–903.
- Mikutta, R., Turner, S., Schippers, A., Gentsch, N., Meyer-Stuve, S., Condron, D.A., Peltzer, D.A., Richardson, S.J., Eger, A., Hempel, G., Kaiser, K., Klotzbucher, T., Guggenberger, G., 2019. Microbial and abiotic controls on mineral-associated organic matter in soil profiles along an ecosystem gradient. Sci. Rep. 9, 10294.
- Pan, W., Kan, J., Inamdar, S., Chen, C., Sparks, D., 2016. Dissimilatory microbial iron reduction release DOC (dissolved organic carbon) from carbon-ferrihydrite association. Soil Biol. Biochem. 103, 232–240.
- Perez-Fodich, A., Derry, L.A., 2019. Organic acids and high soil CO2 drive intense chemical weathering of Hawaiian basalts: Insights from reactive transport models. Geochim. Cosmochim. Acta 249, 173–198.
- Poeplau, C., Don, A., Six, J., Kaiser, M., Benbi, D., Chenu, C., Cotrufo, M.F., Derrien, D., Gioacchini, P., Grand, S., Gregorich, E., Griepentrog, M., Gunina, A., Haddix, M., Kuzyakov, Y., Kühnel, A., Macdonald, L.M., Soong, J., Trigalet, S., Vermeire, M.L., Rovira, P., van Wesemael, B., Wiesmeier, M., Yeasmin, S., Yevdokimov, I., Nieder, R., 2018. Isolating organic carbon fractions with varying turnover rates in temperate agricultural soils a comprehensive method comparison. Soil Biol. Biochem. 125. 10–26.
- Possinger, A.R., Bailey, S.W., Inagaki, T.M., Kögel-Knabner, I., Dynes, J.J., Arthur, Z.A., Lehmann, J., 2020. Organo-mineral interactions and soil carbon mineralizability with variable saturation cycle frequency. Geoderma 375, 114483.
- Rethemeyer, R., Kramer, C., Gleixner, G., Wiesenberg, G.L.B., Schwark, L., Andersen, N., Nadeau, M.J., Grootes, P.M., 2004. Complexity of soil organic matter: AMS 14C analysis of soil lipid fractions and individual compounds. Radiocarbon 46, 465–473.
- Rumpel, C., Kogel-Knabner, I., 2011. Deep soil organic matter-a key but poorly understood component of terrestrial C cycle. Plant Soil 338, 143–158.
- Saatchi, S.S., Harris, N.L., Brown, S., Lefsky, M., Mitchard, E.T.A., Salas, W., Zutta, B.R., Buermann, W., Lewis, S.L., Hagen, S., Petrova, S., White, L., Silman, M., Morel, A., 2011. Benchmark map of forest carbon stocks in tropical regions across three continents. Proc. Natl. Acad. Sci. U. S. A. 108, 9899–9904.
- Sanderman, J., Grandy, S., 2020. Ramped thermal analysis for isolating biologically meaningful soil organic matter fractions with distinct residence times. Soil 6, 131–144.

- Scharlemann, J.P.W., Tanner, E.V.J., Hiederer, R., Kapos, V., 2014. Global soil carbon: understanding and managing the largest terrestrial carbon pool. Carbon Manag. 5, 91, 91
- Schimel, J.P., Wetterstedt, J.A.M., Holden, P.A., Trumbore, S.E., 2011. Drying/rewetting cycles mobilize old C from deep soils from a California annual grassland. Soil Biol. Biochem. 43, 1101–1103.
- Schmidt, M.W.I., Torn, M.S., Abiven, S., Dittmar, T., Guggenberger, G., Janssens, I.A., Kleber, M., Kögel-Knabner, I., Lehmann, J., Manning, D.A.C., Nannipieri, P., Rasse, D.P., Weiner, S., Trumbore, S.E., 2011. Persistence of soil organic matter as an ecosystem property. Nature 478, 49–56.
- Schrumpf, M., Kaiser, K., Guggenberger, G., Persson, T., Kögel-Knabner, I., Schulze, E.-D., 2013. Storage and stability of organic carbon in soils as related to depth, occlusion within aggregates, and attachment to minerals. Biogeosciences 10, 1675–1691.
- Shi, Z., Allison, S.D., He, Y., Levine, P.A., Hoyt, A.M., Beem-Miller, J., Zhu, Q., Wieder, W.R., Trumbore, S., Randerson, J.T., 2020. The age distribution of global soil carbon inferred from radiocarbon measurements. Nat. Geosci. 13, 555–559.
- Shoji, S., Nanzyo, M., Shirato, Y., Ito, T., 1993. Chemical-kinetics of weathering in young andisols from northeastern Japan using soil age normalized to 10-degrees-c. Soil Sci. 155, 53–60.
- Sierra, C.A., Müller, M., Metzler, H., Manzoni, S., Trumbore, S.E., 2017. The muddle of ages, turnover, transit, and residence times in the carbon cycle. Glob. Chang. Biol. 23, 1763–1773.
- Spengler, S.R., Garcia, M.O., 1988. Geochemistry of the Hawi lavas, Kohala Volcano, Hawaii. Contrib. Mineral. Petrol. 99, 90–104.
- Stuiver, M., Polach, H.A., 1977. Reporting of C-14 data discussion. Radiocarbon 19, 355–363.
- Su, H., Jiang, J.H., Neelin, J.D., Shen, T.J., Zhai, C., Yue, Q., Wang, Z., Huang, L., Choi, Y.-S., Stephens, G.L., Yung, Y.L., 2017. Tightening of tropical ascent and high clouds key to precipitation change in a warmer climate. Nat. Commun. 8, 15771.
- Synal, H.A., Stocker, M., Suter, M., 2007. MICADAS: a new compact radiocarbon AMS system. Nucl. Instrum. Methods Phys. Res., Sect. B 259 (1), 7–13.
- Teutsch, N., Erel, Y., Halicz, L., Chadwick, O.A., 1999. The influence of rainfall on metal concentration and behavior in the soil. Geochim. Cosmochim. Acta 63, 3499–3511.
- Thompson, A., Chadwick, O.A., Boman, S., Chorover, J., 2006a. Colloid mobilization during soil iron redox oscillations. Environ. Sci. Technol. 40, 5743–5749.
- Thompson, A., Chadwick, O.A., Rancourt, D.G., Chorover, J., 2006b. Iron-oxide crystallinity increases during soil redox oscillations. Geochim. Cosmochim. Acta 70, 1710–1727.
- Thompson, A., Rancourt, D.G., Chadwick, O., Chorover, J., 2008. Evolution of soil Iron mineral composition as a function of climate-driven Fe loss. Geochim. Cosmochim. Acta 72. A946.
- Thompson, A., Rancourt, D.G., Chadwick, O.A., Chorover, J., 2011. Iron solid-phase differentiation along a redox gradient in basaltic soils. Geochim. Cosmochim. Acta 75, 119–133.
- Torn, M.S., Trumbore, S.E., Chadwick, O.A., Vitousek, P.M., Hendricks, D.M., 1997.

  Mineral control of soil organic carbon storage and turnover. Nature 389, 170–173.
- Trumbore, S.E., 1997. Potential responses of soil organic carbon to global environmental change. Proc. Natl. Acad. Sci. U. S. A. 94, 8284–8291.
- Trumbore, S., 2009. Radiocarbon and soil carbon dynamics. Annu. Rev. Earth Planet. Sci. 37, 47–66.
- van der Voort, T.S., Zell, C.I., Hagedorn, F., Feng, X., McIntyre, C.P., Haghipour, N., Pannatier, E.G., Eglinton, T.I., 2017. Diverse soil carbon dynamics expressed at the molecular level. Geophys. Res. Lett. 44, 11840–11850.
- van der Voort, T.S., Mannu, U., Hagedorn, F., McIntyre, C., Walthert, L., Schleppi, P., Haghipour, N., Eglinton, T.I., 2019. Dynamics of deep soil carbon—insights from <sup>14</sup>C time series across a climatic gradient. Biogeosciences 16, 3233–3246.
- Vitousek, P.M., Chadwick, O.A., 2013. Pedogenic thresholds and soil process domains in basalt-derived soils. Ecosystems 16, 1379–1395.
- Vitousek, P.M., Chadwick, O.A., Crews, T.E., Fownes, J.H., Hendricks, D.M., Herbert, D., 1997. Soil and ecosystem development across the Hawaiian Islands. GSA Today 7, 1–8.
- Wacker, L., Bonani, G., Friedrich, M., Hajdas, I., Kromer, B., Nemec, M., Ruff, M., Suter, M., Synal, H.A., Vockenhuber, C., 2010. MICADAS: routine and high-precision radiocarbon dating. Radiocarbon 52, 252–262.
- Wang, et al., 1998. Radiocarbon studies of organic compound classes in plankton and sediment of the northeastern Pacific Ocean. Geochim. Cosmochim. Acta 62, 1365–1375.
- Zhao, Q., Adhikari, D., Huang, R., Patel, A., Wang, X., Tang, Y., Obrist, D., Roden, E.E., Yang, Y., 2017. Coupled dynamics of iron and iron-bound organic carbon in forest soils during anaerobic reduction. Chem. Geol. 464, 118–126.

# <u>Update</u>

## **Chemical Geology**

Volume 590, Issue , 20 February 2022, Page

DOI: https://doi.org/10.1016/j.chemgeo.2021.120700



Contents lists available at ScienceDirect

## **Chemical Geology**

journal homepage: www.elsevier.com/locate/chemgeo



## Erratum



# Erratum to 'Persistence of old soil carbon under changing climate: The role of mineral-organic matter interactions' [Chemical Geology 587 (2021) 120629]

Katherine E. Grant <sup>a,\*</sup>, Valier V. Galy <sup>b</sup>, Negar Haghipour <sup>c,d</sup>, Timothy I. Eglinton <sup>c</sup>, Louis A. Derry <sup>a,e</sup>

The publisher regrets to inform that the version of Table 1 available in the previously published version of this article is incorrect. The readers are requested to use the corrected version of Table 1 published

here.

The publisher would like to apologise for any inconvenience caused.

DOI of original article: https://doi.org/10.1016/j.chemgeo.2021.120629.

<sup>&</sup>lt;sup>a</sup> Department of Earth and Atmospheric Sciences, Cornell University, Ithaca, NY 14853, USA

b Department of Marine Chemistry and Geochemistry, Woods Hole Oceanographic Institution, 266 Woods Hole Road, Woods Hole, MA 02543, USA

<sup>&</sup>lt;sup>c</sup> Geological Institute, ETH-Zurich, Zurich, Switzerland

<sup>&</sup>lt;sup>d</sup> Laboratory for Ion Beam Physics, ETH-Zurich, Zurich, Switzerland

<sup>&</sup>lt;sup>e</sup> Institut de Physique du Globe de Paris, France

<sup>\*</sup> Corresponding author.

 Table 1

 Characterization table for Pololu soils in this study.

Site number	Site designation	UTM Zone 5 Northing	UTM Zone 5 Easting	Elevation (m)	Estimated rainfall (mm)	Vegetation	# of horizons collected	Total depth (cm)
1	PL3717	213990	2220073	1133	1678	Pasture	6	79
2	PL3920	214196	2220432	1195	1784	Pasture	6	90
3	PL4169	214528	2220721	1271	1915	Pasture	7	105
4	PL4270	214653	2220851	1301	2000	Pasture	5	90
5	PL4535	214971	2221596	1382	2107	Pasture	8	90
6	PL4625	214897	2221340	1410	2154	Pasture	5	83
7	PL4697	215054	2221386	1432	2192	Pasture	8	93
8	PL4750	214941	2221533	1448	2220	Pasture	7	97
9	PL4763	215050	2221442	1452	2226	Forest	7	95
11	PL4800	214737	2221190	1463	2246	Pasture	7	80
10	PL4782	215145	2221488	1458	2236	Forest	7	65
12	PL4865	215230	2221617	1483	2280	Forest	5	60
13	PL4925	215332	2221715	1501	2311	Forest	5	60
14	PL4990	215379	2221798	1521	2345	Forest	6	67
15	PL5100	215471	2221975	1554	2403	Forest	4	61